Temperature dependent nonlinear response of quantum cascade structures

Winge, David; Wacker, Andreas

Published in:
Optical and Quantum Electronics

DOI:
10.1007/s11082-013-9779-9

Published: 2014-01-01

Noname manuscript No.
(will be inserted by the editor)

Temperature dependent nonlinear response of quantum cascade structures

David O. Winge · Andreas Wacker

Received: date / Accepted: date

Abstract Current response and gain spectrum of a terahertz quantum cascade laser is analyzed at different temperatures by a non equilibrium Green's functions approach. The simulations are compared to recent results of time domain spectroscopy. Being able to retrieve higher harmonics of the response function, nonlinear phenomena in quantum cascade lasers are studied theoretically. For different temperatures, gain is simulated under operating conditions and related to the intensity inside the cavity, showing the degradation of performance with temperature. Resolving the electron densities in energy, shows the breakdown of inversion at high intensities.

Keywords terahertz · quantum cascade lasers · gain simulations · nonlinear response · gain clamping

1 Introduction

The promise of possible coherent radiation in the terahertz range has induced a lot of research in the field of Terahertz Quantum Cascade Lasers [1,2] (THz-QCLs). Possible applications for sources in this frequency range are many, such as imaging [3] and spectroscopy [4]. In order to make these applications reality, compact and convenient systems operating over cryogenic temperatures are a necessity, and currently designs based on resonant phonon extraction [5] are the most promising. To this day they have achieved operating temperatures up to ~ 200 K. [6]

Gain, or negative absorption, is an observable of the QCL that is of utmost importance for its characterization, as it describes the amplification of the optical field in the designed heterostructure material. This quantity has in recent years been successfully measured in detail in Time-Domain-Spectroscopy (TDS) experiments [7,8] where THz-QCLs are probed by ultra short pulses. This method provides information on both phase and amplitude of the transmitted pulse, whereafter the gain spectrum can be reconstructed by a Fourier transform. The pulse

D. O. Winge and A. Wacker
Mathematical Physics, Lund University, Box 118, 22100 Lund, Sweden
E-mail: david.winge@teorfys.lu.se

is made as strong as possible in order to get a good signal to noise ratio but it is not known how the system dynamics is affected by such a measurement, and this is a question that was addressed by us in earlier work [9]. The simulation of THz-QCLs relies on a consistent treatment of tunneling and scattering, either by hybrid density matrix/rate equation schemes [10–14] or more evolved Non-Equilibrium Green's Function (NEGF) theory [15–18]. The model used in this work is an extension of our NEGF scheme towards the treatment of high intensities inside the QCL, going beyond linear response to an external electromagnetic field. A detailed summary of the novel ingredients of the model can be found in [19].

2 Theoretical approach

In order to calculate the gain, one can go beyond linear response using a finite ac field strength. This approach is made in this article as we consider a time-dependent electric field $F(t) = F_{\rm dc} + F_{\rm ac}\cos(\Omega t)$ in the cavity, which reflects both the applied bias ($F_{\rm dc}$) and the electric component ($F_{\rm ac}$) of a monochromatic field of angular frequency Ω in the cavity. This requires the solution of the time-dependent Kadanoff-Baym equation for the lesser and retarded Green's functions, $G^<_{\alpha\beta}(\mathbf{k}, t_1, t_2)$ and $G^{\rm ret}_{\alpha\beta}(\mathbf{k}, t_1, t_2)$, respectively [20]. Here α, β denote the states in growth direction and $\mathbf{k}$ the in-plane momentum due to the translational invariance. The periodicity in time allows for a Fourier decomposition of the Green's functions

$$G(\mathbf{k}; t_1, t_2) = \frac{1}{2\pi}\int \mathrm{d}E \sum_h \mathrm{e}^{-\mathrm{i}E(t_1-t_2)/\hbar} G_h(\mathbf{k}, E)\mathrm{e}^{-\mathrm{i}h\Omega t_1} \tag{1}$$

and similarly for the self-energies. This provides a set of equations for the Green's functions for given self-energies $\Sigma_{\alpha\beta,h}(\mathbf{k}, E)$, which are defined analogously. This procedure follows essentially the concepts outlined in Ref. [21] and details can be found in [19]. Here the terms with $h = 0$ correspond to the stationary transport considered before [15], while the higher order terms take into account the ac field. For the fields considered in this manuscript we used $h = -2, -1, 0, 1, 2$, while checking that increasing the number did not change the results (generally higher values of $|h|$ are required with increasing ratios $\mathrm{e}F_{\rm ac}d/\hbar\Omega$, where d is the period of the QCL structure). Relations to observables are made through the $h = 0$ and $h = 1$ components although the higher orders effect the lower ones implicitly. The Green's functions allow for a determination of the current, where $G^<_{\alpha\beta\,h}(\mathbf{k}, E)$ provides the dc current for $h = 0$ and the ac current with frequency Ω for $h = 1$. Dividing the latter by $F_{\rm ac}$ provides the conductivity, directly related to the gain coefficient.

The Hamiltonian for our system can be formulated as

$$H(t) = \underbrace{T + V_{HS} + V(t)}_{H_0} + H^{\rm scatt} \tag{2}$$

where T is the kinetic energy, V_{HS} the heterostructure potential and $V(t)$ the applied field. The scattering mechanisms contained in $H^{\rm scatt}$ in the QCL will break the translational invariance, i.e. couple states with different values of $\mathbf{k}$. The parts of the Hamiltonian describing these mechanisms will thus be non-diagonal in $\mathbf{k}$. In H_0 we put things that are diagonalizable in the basis of Wannier functions

(or any other set of basis states in the growth direction z). As seen in Eq. (2), this consists of the potential of the heterostructure V_{HS} added to the electric field applied to the structure – both a static (dc) and a varying (ac) electromagnetic field, as well as the kinetic energy of the electrons.

We include a number of different self energies to account for the scattering mixing states with different $\mathbf{k}$. The impurity scattering self-energy arises from the dopant atoms in the lattice. Every dopant atom slightly changes the electronic potential locally, and can thus scatter electrons elastically. The same mechanism can also be used in explaining the interface roughness scattering. In this case, the boundaries of the layers are most probable not entirely sharp and this will again produce a local defect in the conduction band. Moreover we have alloy scattering also contributing as a static effect and comes from the fact that two materials (with different band structure) are mixed. The optical and acoustic phonon self-energies give the inelastic scattering in the QCL. A detailed description on how these self-energies are implemented in our model can be found in Ref. [19], Appendix B.

The inelastic scattering is central for a temperature analysis of a QCL. As it is the only way for electrons to relax, it will totally govern the way the electrons thermalize. In this context, one should also emphasize that the optical phonon scattering is the fastest scattering mechanism in a system like the terahertz-QCL. In our model, we treat the acoustic and optical phonons separately. Both distributions are considered to be thermalized, in contrast to the nonequilibrium distribution considered for the electrons. They are treated as thermalized Boltzmann distributions, giving higher probability for higher energy states in these distributions to be occupied as temperature increases. The concept of *temperature* in this work will be the temperature of the phonon distribution which is just the lattice temperature. It has actually been shown that nonequilibrium phonon distributions occur in related devices [22]. Such effects are treated here by assuming an increased lattice temperature compared to the heatsink.

3 Simulation results

In this work we simulate the nonlinear response of a structure recently studied in [8]. The design is a four well structure, exploiting the quick optical phonon scattering in order to achieve efficient depopulation of the lower laser state, a so called resonant-phonon design. One period of this structure is shown in Fig. 1 together with calculated electron densities resolved in growth direction z and energy E. In the same figure the spectral function corresponding to the five most important states for transport is also shown. The total spectral function is not shown, rather lines at energies corresponding to a maximum in the density of states, projected down to look more like states. The states 1' and 2' belong to the left neighboring period, and the lasing is indicated by a white arrow from state 5 to 4. The quick emptying of state 4 is facilitated by scattering via state 3 to 1 by a longitudinal optical phonon at about $\hbar\omega_{LO} = 36.7$ meV.

Results regarding this structure have been presented by us earlier [9], where we showed how the gain and transport properties change under irradiation at intensities both below and over the estimated level of operation. Here, we would like to focus on the degradation in performance with rising temperature, to show the flexibility of our nonequilibrium Green's function model.

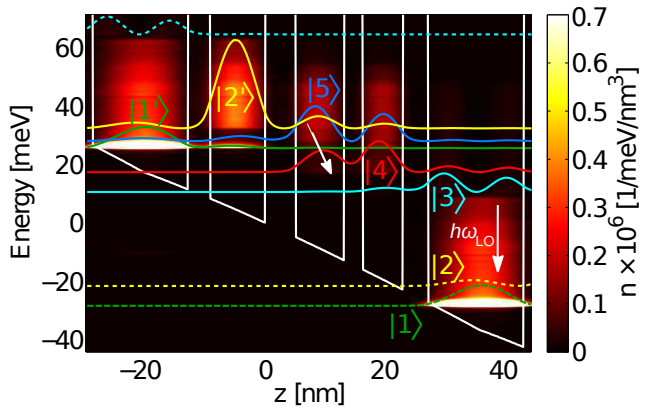

Fig. 1 Calculated electron densities at 10K and a dc bias of 54 mV per period resolved in position and energy are shown in the colormap. Also plotted are selected parts of the spectral function at $\mathbf{k}$=0, $A_{\alpha\beta}(\mathbf{k}=0,E) = i(G^{>}_{\alpha\beta}(\mathbf{k}=0,E) - G^{<}_{\alpha\beta}(\mathbf{k}=0,E))$ for energies E corresponding to the maxima of $A(\mathbf{k}=0,E)$. The lasing transition is between state 5 and 4.

Current response to a static bias (dc) is shown in Fig. 2 for different lattice temperatures together with experimental results. The heatsink temperature for the measurements was reported to be $\sim$ 33K, and that would imply a lattice temperature being slightly higher. There is a good qualitative correspondence in the current at these low temperatures, where we have a current peak at the correct position and are within a 20% margin of the peak value. With increasing temperature, phonon assisted transitions become more probable, opening up new ways of transport. On the other hand, hot–or smeared out, electron distributions will be less sensitive to precisely engineered tunnel transitions. Thus a battle of these two effects is expected, and this can be seen by again studying Fig. 2. At 10K we see sharp current peaks, but this effect gets less important at higher temperatures in favor of a more smooth current-voltage behavior. Overall, the increase of channels available for transport proves the most important effect, increasing the current with temperature. A main feature of the low temperature behavior in Fig. 2 is the pre-peak at around 40 mV per period. It has, as seen in the figure, no connection to the experimental data, and we consider it an artefact of the model. It arises from a long range tunneling transition across an entire period, and we currently attribute this effect to the neglect of electron-electron scattering. A more efficient dephasing of the coherent current carrying states, shown in [15], would be able to counter this effect, and we see that at higher temperatures, the long range tunneling becomes less important as dephasing is more efficient due to enhanced phonon scattering.

For all temperatures studied in Fig. 2 the gain spectra are analyzed at a common operation point. This is chosen to be at 54 mV per period as this corresponds to a high current for all temperatures without entering the region of negative differential resistance. The results of the gain simulations are displayed in Fig. 3(a) and here the degradation of the laser performance with temperature is evident. At low temperature a gain peak at 4 meV can also be observed. This is probably

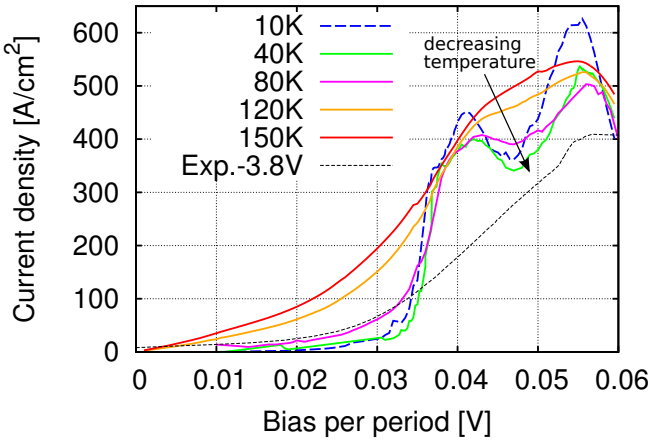

Fig. 2 Current-voltage characteristics at different lattice temperatures. Experimental data from [8] is shown with an assumed contact drop of 3.8V and a reported heatsink temperature of $\sim$ 33K.

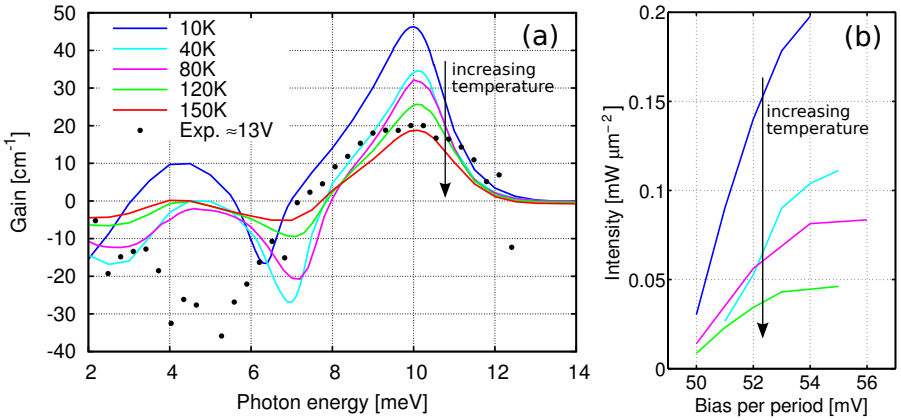

Fig. 3 (a) Gain simulations at different temperatures for a dc bias of 54 mV/period. Experimental data from Ref. [8] are again shown. It is measured at a bias corresponding to 53 mV/period with the contact drop of 3.8V again taken into account. The heatsink temperature was again $\sim$ 33K. (b) Calculated optical intensity inside the cavity for different temperatures (colors correspond to the same temperatures as in (a)). The photon energy was set to $\hbar\omega = 10$ meV.

an inversion effect between state 2 and 5, and this can actually be studied in the electron density plot of Fig. 1.

The strong gain peak is quickly saturated with increasing temperature and between 120K and 150K it drops below 18 cm^{-1}; which is the measured level of losses for the waveguide reported in [8]. The estimate that lasing would stop around these temperatures agrees roughly with studies done by B.S. Williams *et al.* [23] on a similar design, reporting lasing up to a heatsink temperature of 72K, which would correspond to a lattice temperature of at least 100K.

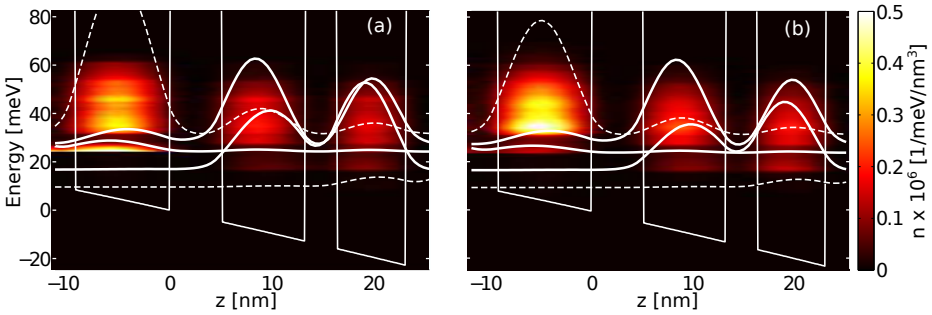

Fig. 4 Close up on the inversion situation between states injector state 1', upper laser state 5 and lower laser state 4. The dc bias was 54 mV per period and the temperature is 40K. A clear decrease in population of the two upper states can be seen and explains the decrease of gain from 32 cm^{-1} at an ac field intensity of 6 μW $\mu\mathrm{m}^{-2}$ (a), to 13 cm^{-1} at a field intensity of 0.2 mW $\mu\mathrm{m}^{-2}$ (b). Also seen in the upper left side of the plots is state 2' of the lefthand period as well as the extraction state (around 10 meV).

In a lasing situation the gain is above the level of the losses. This leads to an enhancement of the ac field inside the cavity, and the increasing intensity will drain the upper laser state of carriers due to stimulated emission. The gain is thus gradually destroyed by the increasing field strength until it is again below the level of the losses. In such a situation the lasing stops, giving the upper laser state time to recover and refill itself with carriers. The forces building up and destroying inversion will thus have one stable point only, which is just at the level of the losses, where the intensity will stabilize. This phenomena is most often referred to as *gain clamping*.

An effect of high intensities can be seen when the theoretical predictions are compared to the measured gain in Fig. 3. The data that best relate to the experiment are the simualtions at 40K and 80K. Here we see a good agreement at photon energies between 8 and 12 meV. Around the laser frequency however, the experimental peak is cut off compared to its simulated counterparts. This is due to the fact that the laser is measured in an on-state, where the gain has already settled at the clamping level and the gain around the laser frequency is thus saturated due to the high intensity of the ac field.

The gain clamping can be used to reconstruct the ac field inside the cavity. Such calculations have been made and are shown in Fig. 3(b). If the system is in a configuration capable of producing gain above the level of the losses, then lasing will start. However, we know that it will stabilize at that level, so we can tune the ac field strength in order to saturate the inversion until the gain reaches this stable point. This will occur at different field strengths for different dc bias and temperatures, yielding the data shown in Fig. 3(b). When calculating the ac field strength at this on-state of the laser, it is also possible to extract the laser driven current contribution, as shown by us earlier in [9]. This provides the opportunity to model the on- and off-state of quantum cascade laser on the same premises.

Saturation of the gain is an effect of stimulated emission. At a high ac field strength at the lasing frequency, there are many photons inducing transitions from the upper to the lower laser state. This effect is visualized in Fig. 4 where a situation with low intensity is compared to the saturated case. Both plots show

data at the same bias point, only the ac field strength is changed. It is clear that the inversion is mostly destroyed and the system is now in a situation far below the level of the losses.

4 Concluding remarks

This work shows the flexibility of our implementation of the nonequilibrium Green's functions. By including higher harmonic components in the expansion of the Green's functions and self energies, nonlinear response simulations can be made. In these calculations, we can look at effects on the gain from changes in bias, field strength and temperature simultaneously. Other tools for diagnostics are the current both for the on- and off-state and the information of the energy resolved densities of the electronic states as shown in Figs. 1 and 4.

Acknowledgements We thank Dayan Ban for helpful discussions and for providing the experimental data of Ref. [8]. Financial support from the Swedish Research Council (VR) is gratefully acknowledged.

References

1. R. Köhler, A. Tredicucci, F. Beltram, H.E. Beere, E.H. Linfield, A.G. Davies, D.A. Ritchie, R.C. Iotti, F. Rossi, Nature **417**, 156 (2002)
2. B.S. Williams, Nature Phot. **1**, 517 (2007).
3. J. Darmo, V. Tamosiunas, G. Fasching, J. Kröll, K. Unterrainer, M. Beck, M. Giovannini, J. Faist, C. Kremser, P. Debbage, Opt. Express **12**(9), 1879 (2004).
4. H.W. Hübers, S.G. Pavlov, H. Richter, A.D. Semenov, L. Mahler, A. Tredicucci, H.E. Beere, D.A. Ritchie, Appl. Phys. Lett. **89**(6), 061115 (2006).
5. B.S. Williams, S. Kumar, H. Callebaut, Q. Hu, J.L. Reno, Appl. Phys. Lett. **83**(25), 5142 (2003).
6. S. Fathololoumi, E. Dupont, C. Chan, Z. Wasilewski, S. Laframboise, D. Ban, A. Mátyás, C. Jirauschek, Q. Hu, H.C. Liu, Opt. Express **20**(4), 3866 (2012).
7. J. Kröll, J. Darmo, S.S. Dhillon, X. Marcadet, M. Calligaro, C. Sirtori, K. Unterrainer, Nature **449**, 698 (2007).
8. D. Burghoff, T.Y. Kao, D. Ban, A.W.M. Lee, Q. Hu, J. Reno, Appl. Phys. Lett. **98**, 061112 (2011).
9. D.O. Winge, M. Lindskog, A. Wacker, Applied Physics Letters **101**(21), 211113 (2012).
10. H. Callebaut, Q. Hu, J. Appl. Phys. **98**, 104505 (2005)
11. S. Kumar, Q. Hu, Phys. Rev. B **80**(24), 245316 (2009).
12. R. Terazzi, J. Faist, New Journal of Physics **12**(3), 033045 (2010)
13. E. Dupont, S. Fathololoumi, H.C. Liu, Phys. Rev. B **81**(20), 205311 (2010).
14. I. Bhattacharya, C.W.I. Chan, Q. Hu, Appl. Phys. Lett. **100**(1), 011108 (2012).
15. S.C. Lee, F. Banit, M. Woerner, A. Wacker, Phys. Rev. B **73**, 245320 (2006)
16. T. Schmielau, M. Pereira, Appl. Phys. Lett. **95**, 231111 (2009)
17. T. Kubis, C. Yeh, P. Vogl, A. Benz, G. Fasching, C. Deutsch, Phys. Rev. B **79**, 195323 (2009)
18. G. Haldaś and, A. Kolek, I. Tralle, Quantum Electronics, IEEE Journal of **47**(6), 878 (2011).
19. A. Wacker, M. Lindskog, D. Winge, Selected Topics in Quantum Electronics, IEEE Journal of, in press (2013). DOI 10.1109/JSTQE.2013.2239613
20. H. Haug, A.P. Jauho, *Quantum Kinetics in Transport and Optics of Semiconductors* (Springer, Berlin, 1996)
21. T. Brandes, Phys. Rev. B **56**, 1213 (1997).
22. M.S. Vitiello, R.C. Iotti, F. Rossi, L. Mahler, A. Tredicucci, H.E. Beere, D.A. Ritchie, Q. Hu, G. Scamarcio, Applied Physics Letters **100**(9), 091101 (2012).
23. B. Williams, S. Kumar, Q. Hu, J. Reno, Electronics Letters **40**, 431 (2004)